Electronic Supplementary Material

Fast adsorption and kinetic separation of benzene and cyclohexane/cyclohexene in a microporous metal azolate framework

Ze-Hao Qiu†, Jing-Hong Li†, Bai-Xun He, Pei-Qin Liao, Mu-Yang Zhou, Pei-Xian Li, Rui-Biao Lin*, Jie-Peng Zhang* and Xiao-Ming Chen

MOE Key Laboratory of Bioinorganic and Synthetic Chemistry, School of Chemistry, IGCME, Sun Yat-Sen University, Guangzhou 510275, China.
Emails: linruibiao@mail.sysu.edu.cn; zhangjp7@mail.sysu.edu.cn.
†These authors contribute equally.

1. Experimental and Computational Simulations Details

1.1. Materials and Measurements

All commercially available reagents and solvents were used without further purification. Benzene, cyclohexane, and cyclohexene were of GC grade, while *n*-hexane was of HPLC grade. The mass spectra (ESI-MS) were collected using the LTQ Orbitrap Elite LC/MS equipment with MeOH as the mobile phase. the powder X-ray diffraction (PXRD) patterns were obtained in reflectance mode using the Bruker D8 ADVANCE X-ray powder diffractometer (Cu Kα) with a step of 0.02° and 10° min^{-1} scan rate. Thermogravimetric (TG) analysis curves were collected under a nitrogen atmosphere using the TGA55 thermogravimetric analyzer at a heating rate of 10 ℃ min^{-1}. Differential scanning calorimetry (DSC) measurements were on a TA DSC 250 instrument. Before measurement, approximately 5 mg of the degassed sample was soaked in corresponding liquid single-components for 30 min and then filtered out and subjected to nitrogen purging at 30 °C (20 mL min^{-1}) for about 10 minutes to remove surface solvent. The system was first cooled down to below 10 ℃, followed by ramping at a rate of 10 ℃ min^{-1}. Gas adsorption isotherms were collected using either the Micromeritics ASAP 2020M or BELSORP max II adsorption instruments, with testing temperatures controlled by a liquid nitrogen bath (77 K) or a water bath (298 K). Prior to adsorption testing, the solvent-exchanged samples were activated by placing them in a sample tube under vacuum heating (100 ℃) for 5 hours. Vacuum degassing was performed on a BSD-VD12 programmable ramping vacuum degasser from Basi Instruments. Gas chromatography-mass (GC-MS) testing used an Agilent 7890A-5975C, Agilent CP-Sil 5CB (CP7709) capillary column, with an inlet temperature of 150 ℃, a column temperature of 35 ℃, a flow rate of 1.2 mL·min^{-1}, a split ratio of 30:1, an injection volume of 1.0 μL, a runtime of 3.65 min, a solvent delay time of 2.55 min, and a post-run setting at 150 ℃ for 4 min with a column flow rate of 1.8 mL·min^{-1}.

1.2. Synthesis of 2,6-bis(5-methyl-1*H*-1,2,4-triazol-3-yl)pyridine (H_2(bmtzpy))

The synthesis method for the ligand can be referenced in the literature,[1] but optimizations and changes have been made here. Firstly, 40 mmol of acetamidine hydrochloride was stirred to dissolve in 100 mL of ethanol, while 40 mmol of sodium ethoxide was stirred to dissolve in 60 mL of ethanol. The two solutions were combined and stirred at 50 °C for 1 hour. The resulting mixture was filtered to remove precipitates, yielding a filtrate.

Secondly, 10 mmol of pyridine-2,6-dicarbohydrazide was added to the filtrate obtained above. The mixture was heated and stirred at reflux (approximately 12-24 hours) until the solution clarified at 120 °C and 800 rpm. Most of the solvent was removed through rotary evaporation. Then, 5 mL of hydrochloric acid was added to induce acidification and precipitation. The precipitate was washed several times with acetonitrile and recrystallized from water (evaporated to approximately 15 mL), further washed with acetonitrile, and dried at 70°C for several hours to yield a white powder (yield ~67%). Mass spectrometry (ESI) in positive ion mode showed m/z = 242 ($[M+H]^+$), 264 ($[M+Na]^+$), and in negative ion mode m/z = 240 ($[M-H]^-$) (Figure S1), M.W.: 241.26.

1.3. Synthesis of MAF-67·guest (MAF-67·g)

Large-particle sample: $Zn(OAc)_2·2H_2O$ (5 mg, 0.02 mmol) and H_2(bmtzpy) (12 mg, 0.05 mmol) were placed into a high-pressure reaction vessel (15 mL) along with 3 mL of methanol and 3 mL of concentrated ammonia aqueous. The mixture was sonicated for 10 minutes until complete dissolution, then left to react in an oven at 160 °C for 24 hours. After slowly cooling to room temperature, transparent block-shaped crystals were obtained for single-crystal X-ray diffraction and structural analysis.

Small-particle sample: $Zn(OAc)_2·2H_2O$ (0.88 g, 4 mmol) and H_2(bmtzpy) (0.96 g, 4 mmol) were added to a thick-walled pressure-resistant bottle (120 mL) with 30 mL of ethanol, 30 mL of water, and 10 mL of concentrated ammonia aqueous. The vessel was sealed and stirred at 120 °C, 800 rpm for 12 hours, resulting in yellowish powder (yield: 86%).

1.4. Synthesis of MAF-67·1/3(C_6H_6)

MAF-67·1/3(C_6H_6) single crystal sample: Apart from adding an additional 0.1 mL of benzene to the solvents, the procedure was consistent with the synthesis method for the MAF-67·g single crystal sample.

1.5. Crystallography

The single-crystal X-ray diffraction (SCXRD) data of MAF-67·g and MAF-67·1/3(C_6H_6) was collected at 150 K in a nitrogen atmosphere using the XtaLAB Synergy R (Cu Kα) diffractometer. All structures were solved by the direct method and refined with the full-matrix least-squares technique on F^2 by the SHELXTL software package in OLEX2. Hydrogen atoms were placed geometrically and anisotropic thermal parameters were applied to all non-hydrogen atoms in the host framework. The hydrogen atoms were generated geometrically. CCDC 2335583-2335584 contains the crystallographic data. These data are provided free of charge from the Cambridge Crystallographic Data Centre via www.ccdc.cam.ac.uk/data_request/cif. Single-crystal data and details of refinements were summarized in Table S1.

1.6. Liquid adsorption measurements

500 μL each of benzene, cyclohexane, and cyclohexene were mixed thoroughly, and then diluted 10,000 times (using *n*-hexane as the solvent) as standard sample (1:1:1) for GC/MS testing. The area ratios obtained for benzene, cyclohexane,

and cyclohexene are 100:68.61(21):74.26(3), with retention times (minutes) of 3.05, 3.22, and 3.54, respectively.

The as-synthesized large-particle sample underwent methanol exchange thrice, was vacuum-filtered, and then subjected to nitrogen purging (20 mL/min) for 30 minutes at room temperature before use in liquid-phase adsorption experiments. The small-particle sample, on the other hand, required five rounds of methanol exchange and a 1-hour vacuum degassing at 400 °C. After cooling to room temperature, the sample was used in the liquid-phase adsorption experiments. The immersion quantity for both samples were approximately 0.2 mL per 1 mg of sample. after specific time of interest, around 5 mg of the sample was filtered out and subjected to nitrogen purging at 30 °C (20 mL min^{-1}) for approximately 10 minutes to remove surface solvent. Approximately 3 mg of the sample was used for TG analysis. The remaining 2 mg of the sample was treated with nitric acid (0.5 mL) and gently shaken until complete dissolution occurred within a few seconds. Then, *n*-hexane (1 mL) was added for extraction, repeated thrice. The collected extract of 3 mL was analyzed using GC-MS to detect benzene, cyclohexane, and cyclohexene component, ensuring that the peak signal intensity does not exceed the upper limit of the detection range. Each sample was measured twice, and the component with the highest content was considered as 100%, while the relative areas of the other components were averaged. The obtained area ratio was divided by the area ratio of the standard sample to determine the volume ratio of benzene, cyclohexane, and cyclohexene. This ratio was multiplied by their respective density ratios (0.874:0.779:0.811 at 25°C) to obtain the mass ratio of the three components. Following this, the adsorption mass ratio of the three components was calculated based on the weight loss from TG analysis, divided by their respective molecular weights, to derive the molar ratio of the adsorbed components and compute the selectivity.

The selectivity of component *b* is defined as:[2] $S_b = \frac{Q_b/(\sum_{i\neq b} Q_i)}{\theta_b/(\sum_{i\neq b} \theta_i)}$, where Q_b is the adsorption capacity of component *b* (mmol g^{-1}), and θ_b is the concentration of *b* in the solution phase.

For the benzene/cyclohexane cyclic adsorption-desorption test, approximately 40 mg of the sample was soaked in a (1:1) mixture of benzene and cyclohexane. After 5 seconds, around 5 mg of the sample was filtered and then subjected to nitrogen gas purging at 30 °C (20 mL min^{-1}) for approximately 10 minutes to remove surface solvent. Approximately 3 mg of the sample was used for thermogravimetric analysis, and 2 mg was used for GC/MS testing. All the remaining samples were subjected to nitrogen purging at 150°C (200 mL min^{-1}) for about 1 hour to remove the guest molecules, preparing them for the next cycle of testing.

1.7. Adsorption Isotherm Measurement

Adsorption/desorption isotherms were measured with automatic volumetric adsorption apparatuses (BELSORP MAX II or ASAP 2020 M). The measurement temperatures were controlled by a liquid-nitrogen bath (77 K). Before the sorption experiments, the samples of MAF-67 (weight of about 100−200 mg) were treated in a dynamic vacuum (stabilized at < 10^{-2} Pa for at least 30 min) for 2 h at 373 K.

1.8. Vapor Adsorption Kinetics Measurement

Single-component Vapor Adsorption Kinetics Characterization was carried out using a fully equipped multi-station gravimetric vapor sorption analyzer from Beishide Instrument Technology Co., Ltd. Before each test, the same sample of **1** (weight of about 200 mg) was purged in situ with nitrogen (mL min^{-1}) and heated to 200 °C for 2 hours. Blank measurements with buoyancy correction were performed for background subtraction.

1.9. Photoluminescence measurement

In-situ time-dependent photoluminescence spectra were measured with an Edinburgh FLS980 single photon counting spectrometer equipped with a continuous xenon lamp and an Andor deep cooling CCD detector. The activated sample of **1** (weight of about 1-2 mg) was attached to a quartz slide and the luminescence spectra without solvent were recorded, then a drop of benzene (about 0.05 mL, far exceeding saturation amount) was carefully added to the sample, and the luminescence spectra were recorded at a time interval of 0.1 s.

1.10. Computational Simulations

All simulations/calculations were performed using the Materials Studio 5.5 package. For periodic density functional theory (PDFT) simulation, the generalized gradient approximation (GGA) with the Perdew-Burke-Ernzerhof (PBE) functional and the double numerical plus d-functions (DNP) basis set, DFT including dispersion correction (DFT-D) with Tkatchenko-Scheffler (TS) method, and the Effective Core Potentials (ECP) were used. The energy, force and displacement convergence criterions were set as 1×10^{-5} Ha, 2×10^{-3} Ha and 5×10^{-3} Å, respectively. The static binding energy (ΔE_B) between guests and host is calculated by: $\Delta E_B = \left|E_{host+guest} - E_{host} - E_{guest}\right|$, where $E_{host+guest}$ is the energy of host with guests adsorbed, E_{host} is the energy of host alone, E_{guest} is the energy of guests.

For Grand Canonical Monte Carlo (GCMC) simulations, the saturation uptakes and gas adsorption sites were generated in a unit cell with the fixed pressure task (at 298 K and corresponding saturated vapor pressure) and fixed loading task (at 298 K and given uptake) in the Sorption module, respectively. The host frameworks and guest molecules were both set flexible. The Metropolis method based on the universal force field (UFF) was used. The Mulliken charges and ESP charges, calculated by PDFT, were employed to the framework atoms and guest atoms, respectively. The cutoff radius was chosen as 12.5 Å for the Lennard-Jones potential, and the electrostatic interactions and van der Waals interactions were handled using the Ewald and Atom based summation methods, respectively. All the equilibration steps and production steps were set as 1×10^7. Before and after GCMC simulations, the host-guest systems were optimized by PDFT simulation.

The classical molecular dynamics (MD) simulations were performed in the Forcite module. The initial configurations for the MD simulations were produced by the GCMC simulation. The host framework and the gas molecule were both regarded as flexible. The simulation box consisted of one unit cell. The cutoff radius was chosen as 15.5 Å for the LJ potential, and the equilibration steps and production steps were both set as 2×10^7. The constant-volume & temperature (NVT) ensemble was used to simulate the dynamic processes and radial distribution function (RDF). The charges and force field are the same with that for GCMC simulations. The electrostatic interactions and the van der Waals interactions were evaluated by the Ewald summation method, with a Buffer width of 0.5 Å. The time step was 1.0 fs with relaxation time 2.0 ps and total simulation time 4 ns. The temperature was 1000 K. The first 2 ns were used as equilibrium and the following 2 ns were adopted for statistical analysis such as for mean square displacements.

2. Analysis of data by Adsorption Kinetics Models

In the study of adsorption kinetics, the intraparticle diffusion of adsorbates (also referred to as intracrystalline diffusion for crystalline materials) and the adsorption reactions at the adsorption sites on the surface of the adsorbent

are often the more focused and frequently assumed processes,[3] commonly used in the literature to represent the kinetics.[4] The slowest step controls the rate of adsorption.

2.1. Adsorption kinetics controlled by diffusion

For intraparticle diffusion in microporous materials (with diameters smaller than 20 Å), surface forces (interaction forces between diffusing molecules and the pore walls) play a dominant role. Adsorbed molecules are always within the force field of the pore walls. Therefore, the fluid in the pores can be considered as a single adsorbed phase. Diffusion is an activated process carried out through a series of jumps between relatively low potential energy regions.[5] If the adsorbent particles are considered spherical, then starting from Fick's second law, the diffusion in micropores satisfies[5]

$$\frac{q(t)}{q_e} = 1 - \frac{6}{\pi^2}\sum_{n=1}^{\infty}\frac{1}{n^2}\exp\left(-\frac{Dn^2\pi^2}{r^2}t\right) \tag{1}$$

with $q(0) = 0$, where D is the self-diffusion coefficient, and r is the particle radius. In the early stages of adsorption ($\frac{q(t)}{q_e} < 0.3$), neglecting higher-order terms, produces:

$$\frac{q(t)}{q_e} = \frac{6}{\sqrt{\pi}}\sqrt{\frac{Dt}{r^2}} \tag{2}$$

Transformed into linear format:

$$\left[\frac{q(t)}{q_e}\right]^2 = \frac{36}{\pi}\frac{D}{r^2}t = \frac{36}{\pi}k_D t \tag{3}$$

Here diffusion time constant is defined as: $k_D \equiv \frac{D}{r^2}$. Linear fitting of $\left(\frac{q_t}{q_e}\right)^2$ against t yields k_D, also obtainable through nonlinear implicit fitting.

2.2. Adsorption kinetics controlled by surface adsorption reactions

In most existing literature on solid-liquid adsorption kinetics, the majority of works have compared the abilities of pseudo-first-order and pseudo-second-order kinetics to describe the data.[4] The following provides a brief description of each.

Pseudo-first order rate law has the original form

$$\frac{\mathrm{d}q(t)}{\mathrm{d}t} = k_1[q_e - q(t)] \tag{4}$$

With the boundary condition of an initial adsorption amount of 0, i.e., $q(0) = 0$, the solution is obtained as:

$$q(t) = q_e[1 - \exp(-k_1 t)] \tag{5}$$

in which $q(t)$ is the adsorption amount at time t, q_e is the equilibrium adsorption amount, and k_1 is the pseudo-first order rate coefficient.

As for Pseudo-second order rate law, the original form is:

$$\frac{\mathrm{d}q(t)}{\mathrm{d}t} = k_2[q_e - q(t)]^2 \tag{6}$$

in which k_2 represents pseudo-second order rate coefficient. With $q(0) = 0$, the solution is

$$q(t) = q_e \frac{k_2^* t}{1 + k_2^* t} \tag{7}$$

where $k_2^* \equiv k_2 q_e$.

2.3. Derivation and Modification Based on Practical Considerations

Due to the gas path switch at the beginning of the gravimetric vapor adsorption test, there is a period during which adsorptive gases rush into the sample chamber. We designate the first recorded point, approximately 1 minute later, as the (t = 0) point. As the sample chamber gradually fills with vapor and approaches saturation, the true time zero point is undefined, failing to meet the boundary condition $q(0) = 0$. This is also the case of the latter stage for kinetics controlled by different adsorption behaviors in distinct stages. However, as the adsorption rates law of the three models only depend on the current state and are independent of the initial state, we propose a modification. We consider that the state at point (t = 0) is equivalent to adsorbing for a time t_{eff}. It is evident that this modification has minimal impact on the solution form of the ordinary differential equation, as shown below.

For intraparticle diffusion, (3) is modified as:

$$\left[\frac{q(t)}{q_e}\right]^2 = \frac{36}{\pi}\frac{D}{r^2}(t + t_{\text{eff}}) = \frac{36}{\pi}k_D(t + t_{\text{eff}}) \tag{8}$$

For Pseudo-first order rate law, (4) and (5) are modified as:

$$\frac{\mathrm{d}q(t)}{\mathrm{d}(t + t_{\text{eff}})} = k_1[q_e - q(t)] \tag{9}$$

$$q(t) = q_e\left[1 - \exp\left(-k_1(t + t_{\text{eff}})\right)\right] \tag{10}$$

For Pseudo-second order rate law, (6) and (7) are modified as:

$$\frac{\mathrm{d}q(t)}{\mathrm{d}(t + t_{\text{eff}})} = k_2[q_e - q(t)]^2 \tag{11}$$

$$q(t) = q_e \frac{k_2^*(t + t_{\text{eff}})}{1 + k_2^*(t + t_{\text{eff}})} \tag{12}$$

3. Figures and Tables

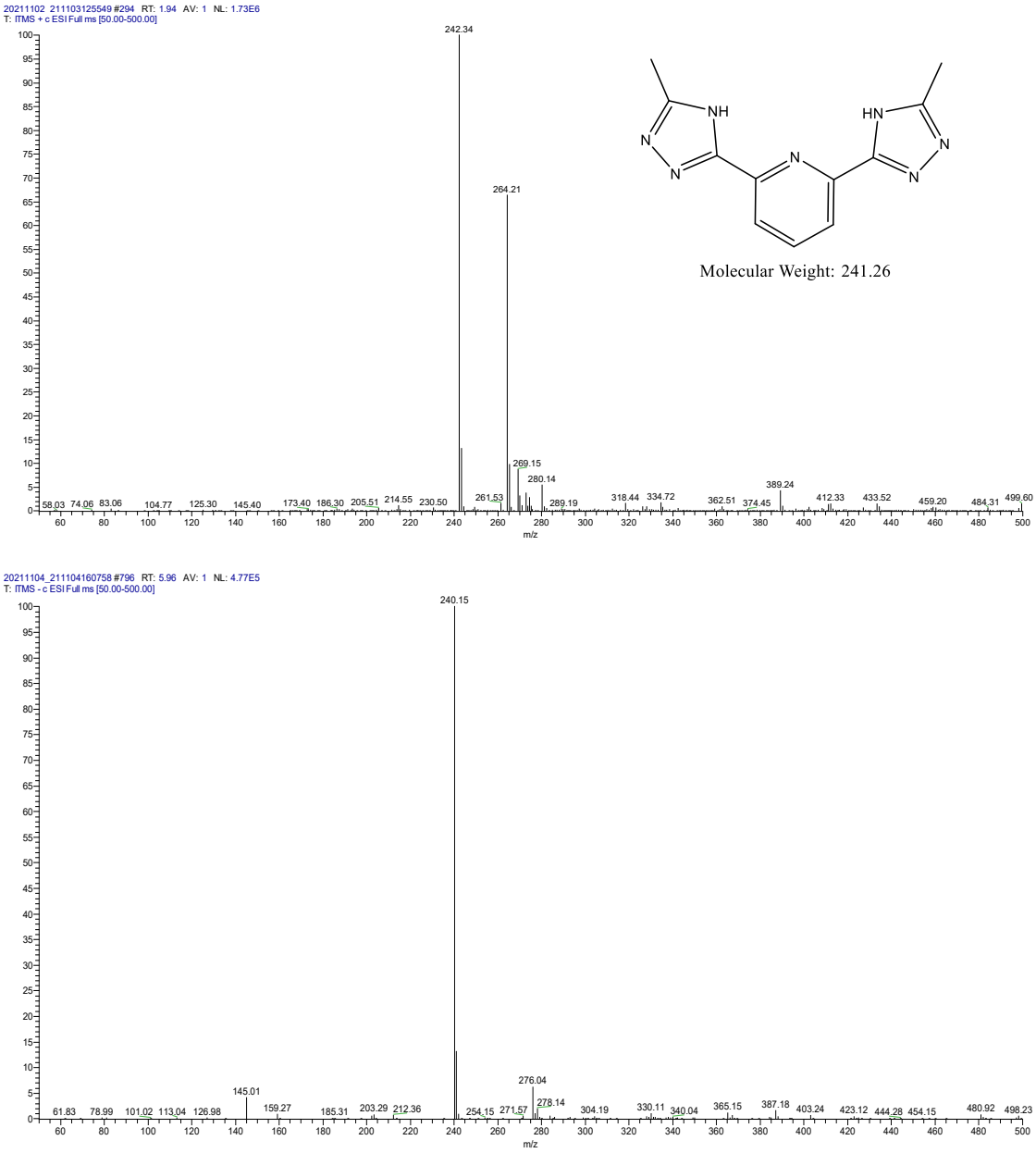

Figure S1. Mass spectrums of organic ligand H_2bmtzpy in (a) positive ion mode and (b) negative ion mode.

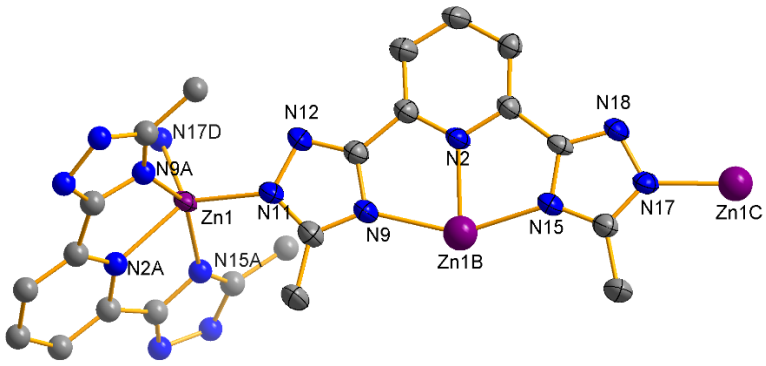

Figure S2. The coordination environment of MAF-67·g. Symmetry codes: A = 1/3+*x*−*y*, −1/3+*x*, 2/3−*z*; B = 1/3+*y*, 2/3−*x*+*y*, 2/3−*z*; C = *x*−*y*, *x*, 1−*z*; D = *y*, −*x*+*y*, 1−*z*. Atoms in the asymmetric unit are drawn with thermal ellipsoids (H atoms on C atoms are omitted for clarify).

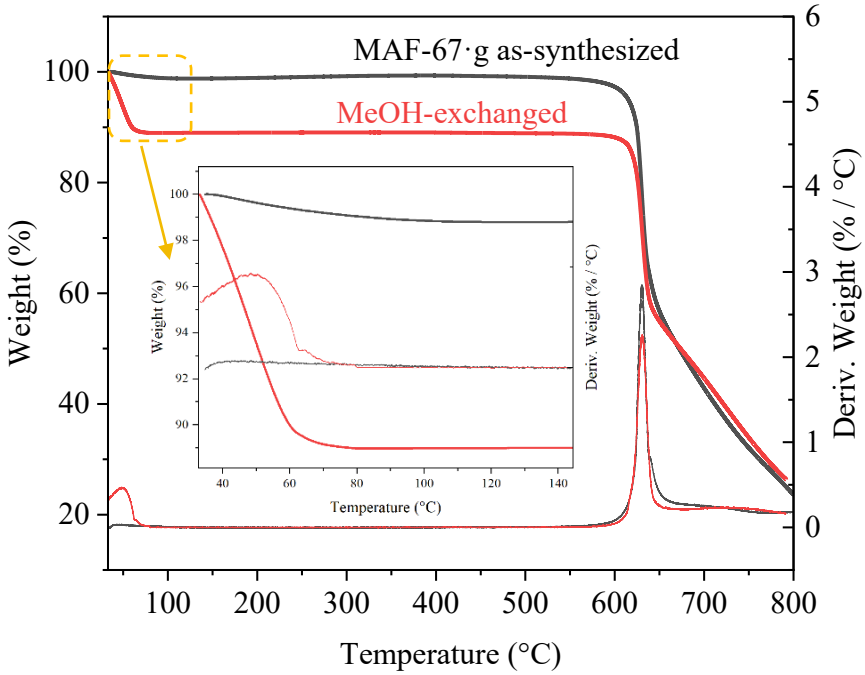

Figure S3. TG Curves of as-synthesized MAF-67·g and the one exchanged with methanol.

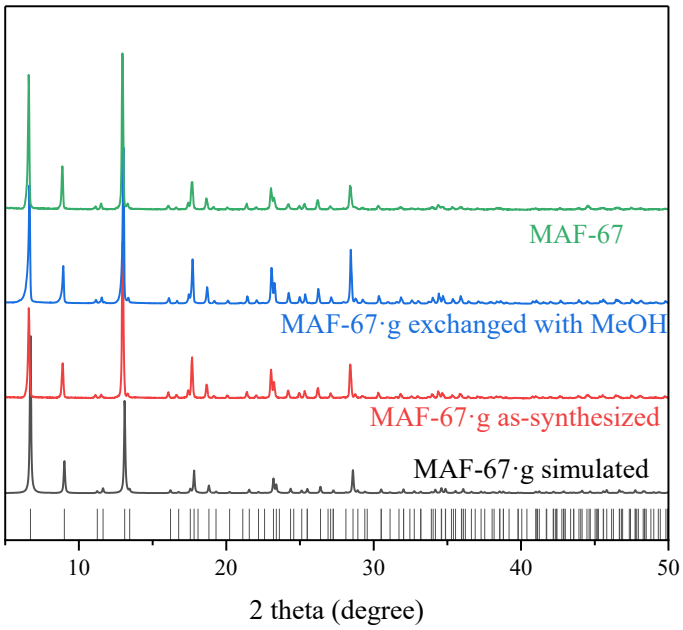

Figure S4. PXRD patterns of as-synthesized MAF-67·g, and the one exchanged with methanol and guest-free MAF-67.

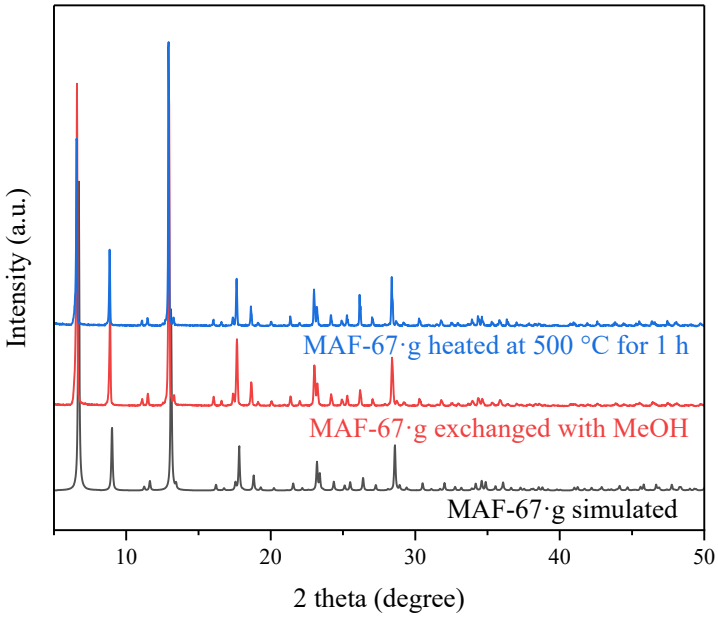

Figure S5. PXRD patterns of MAF-67·g and the one upon heating under nitrogen gas at 500 °C for 1 h.

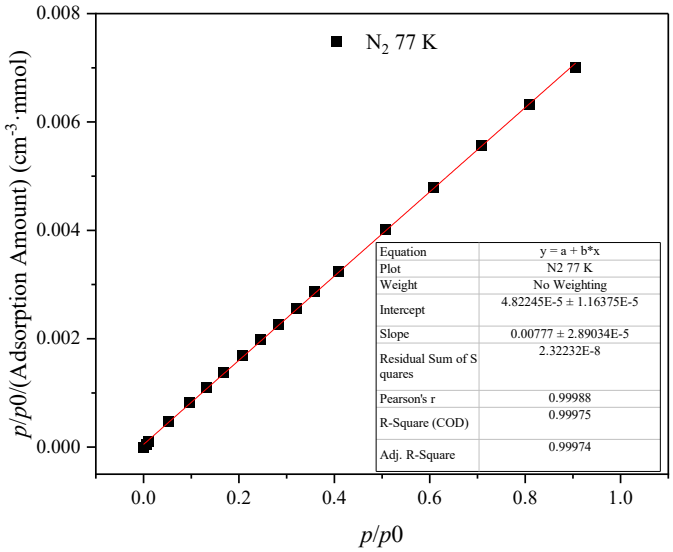

Figure S6. Langmuir linear fitting result of adsorption isotherm for N_2 at 77 K.

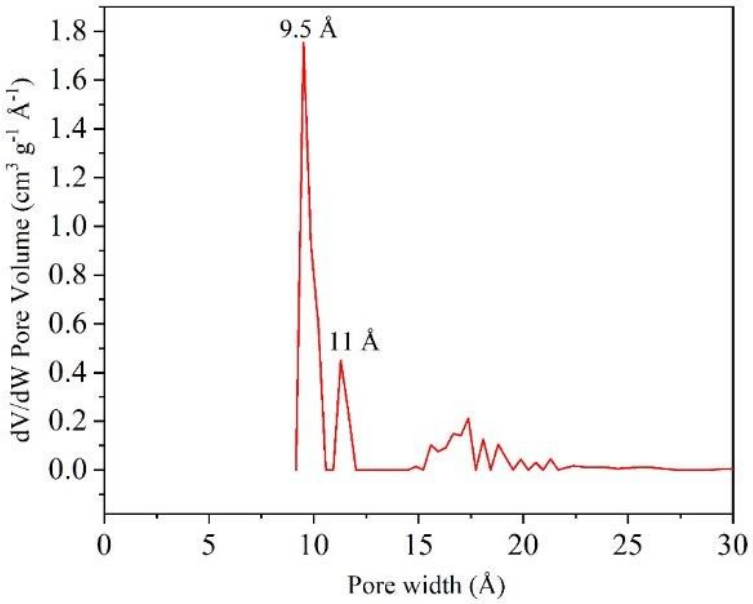

Figure S7. Pore size distribution of MAF-67 calculated from N_2 adsorption isotherm at 77 K.

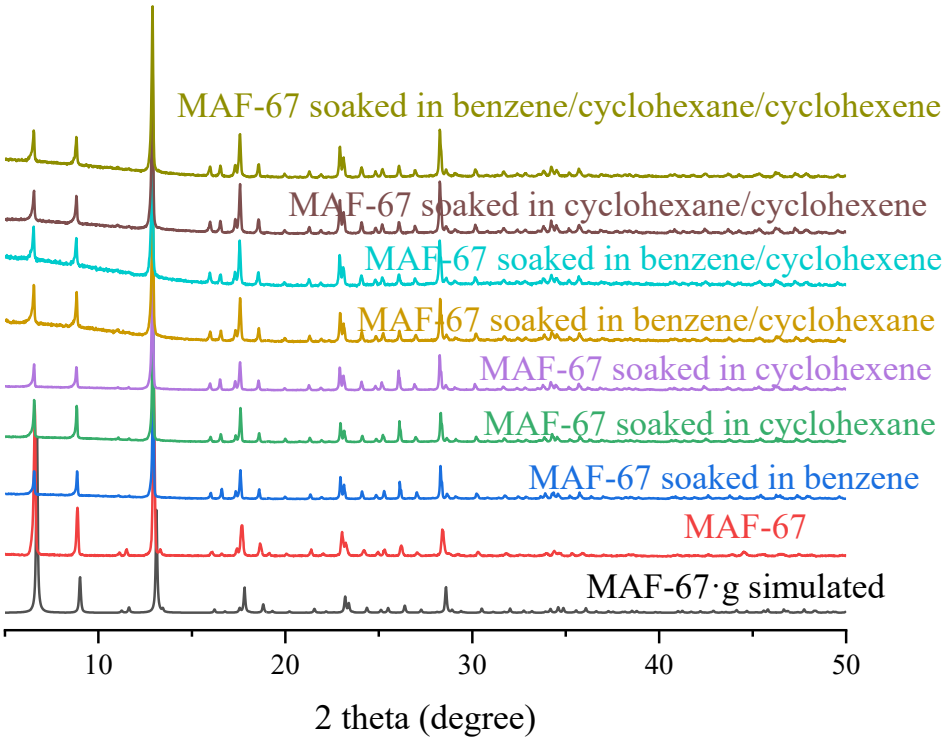

Figure S8. PXRD patterns of MAF-67 after being soaked in single-component or equimolar mixed-component of benzene/cyclohexane/cyclohexene for 2 days.

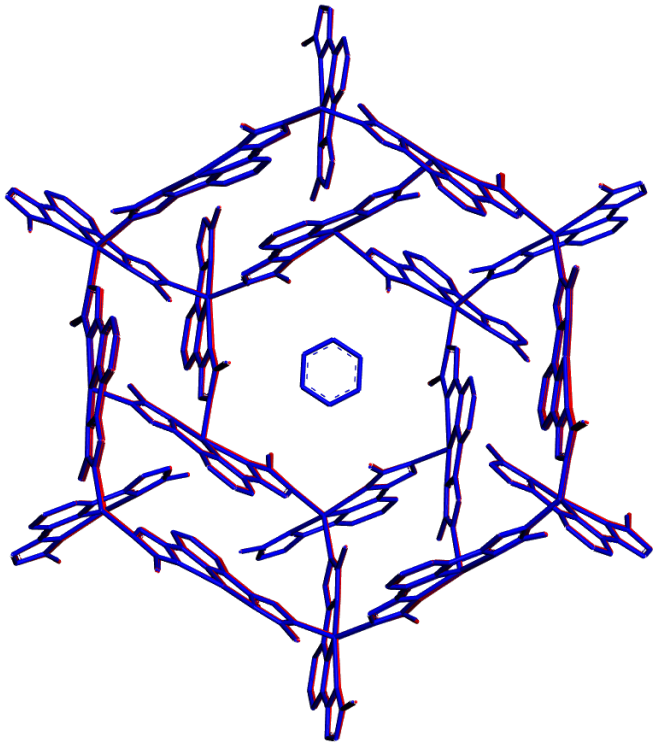

Figure S9. Overlaps of MAF-67·g (red) and MAF-67·1/3(C_6H_6) (blue, some disordered C_6H_6 in the cavity is omitted).

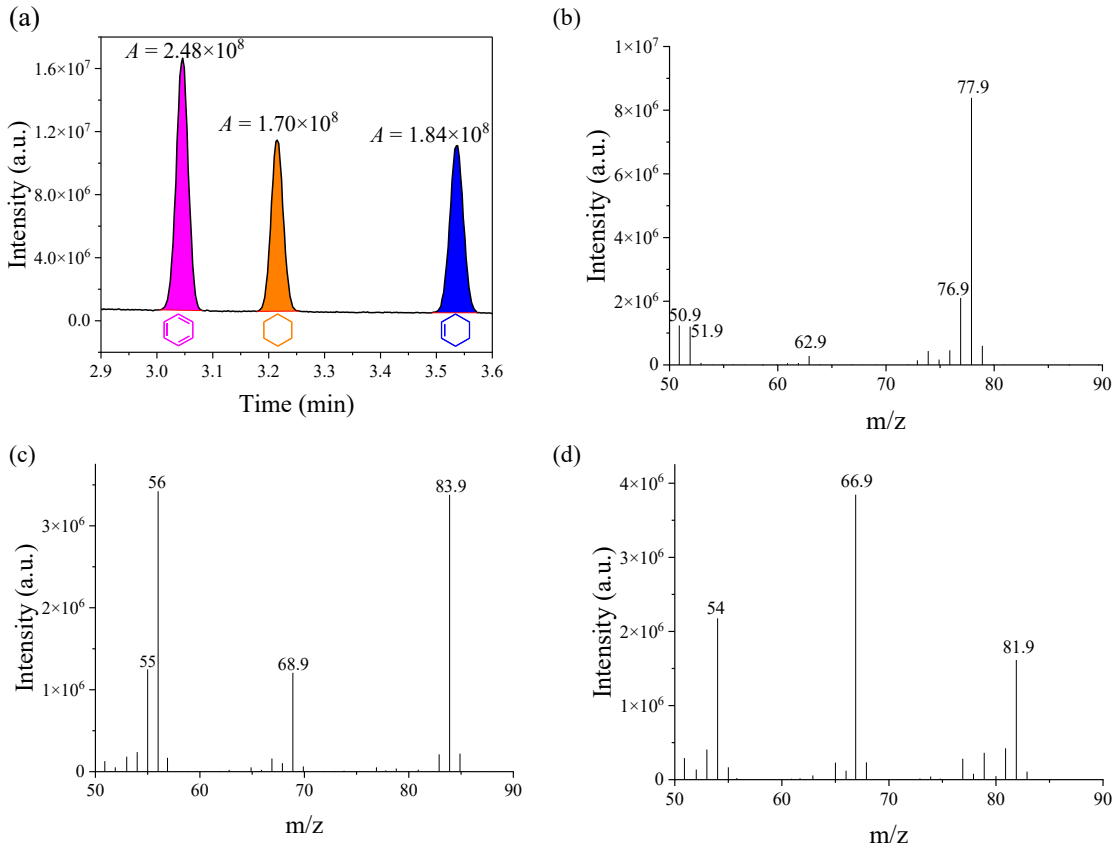

Figure S10. (a) GC-MS spectrum of standard sample benzene:cyclohexane:cyclohexene (volume ratio 1:1:1, diluted with *n*-hexane), with retention times of 3.05, 3.22, and 3.54 min, respectively. Corresponding mass spectrum at (b) 3.05 min, (c) 3.22 min and (d) 3.54 min.

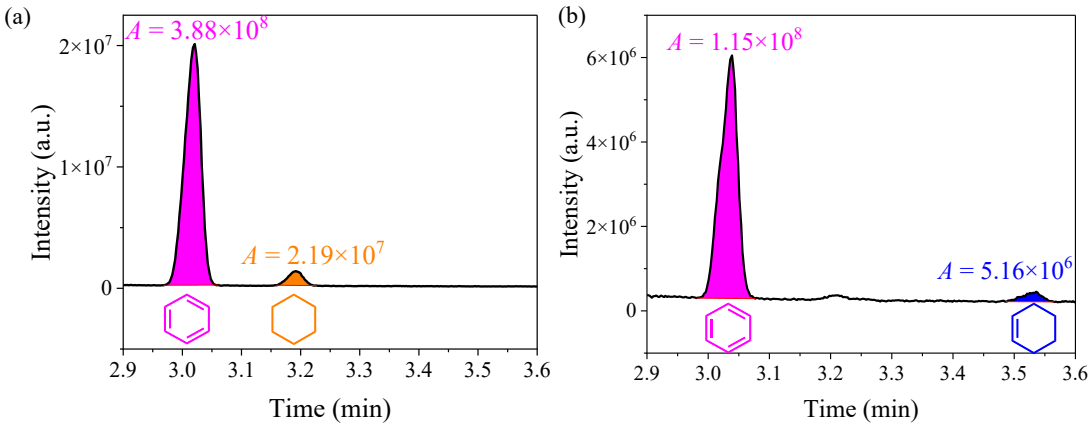

Figure S11. GC spectrum for (a) benzene/cyclohexane and (b) benzene/cyclohexene mixture adsorption.

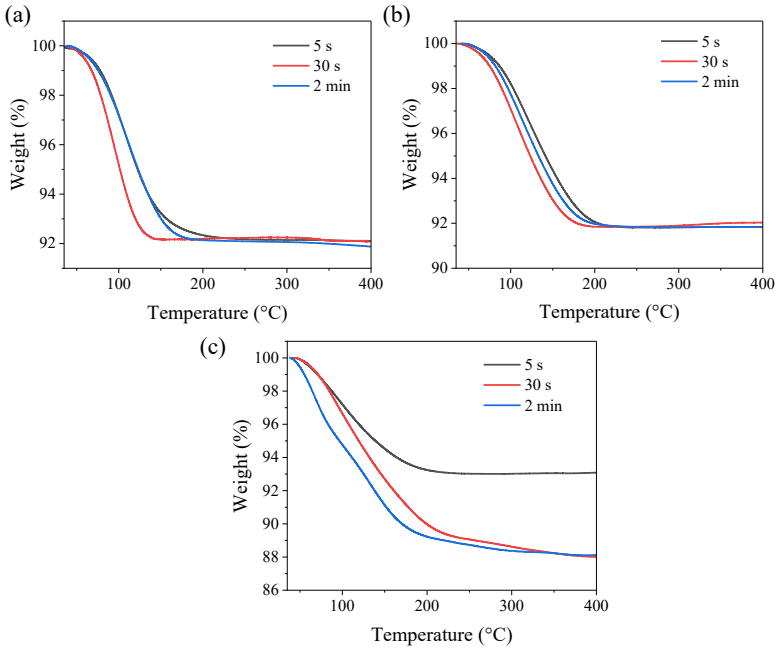

Figure S12. TG Curves of small-particle sample of MAF-67 after soaking in (a) benzene, (b) cyclohexane and (c) cyclohexene.

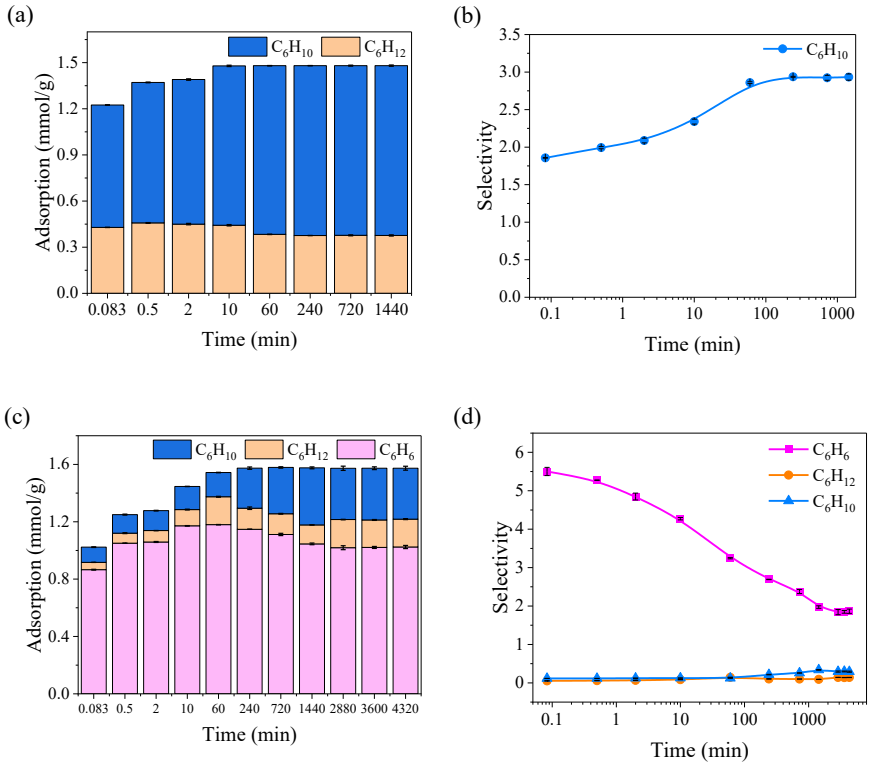

Figure S13. Competitive liquid adsorption kinetics of small-particle MAF-67 for (a-b) cyclohexane/cyclohexene (1:1) and (c-d) benzene/cyclohexane/cyclohexene (1:1:1) mixtures.

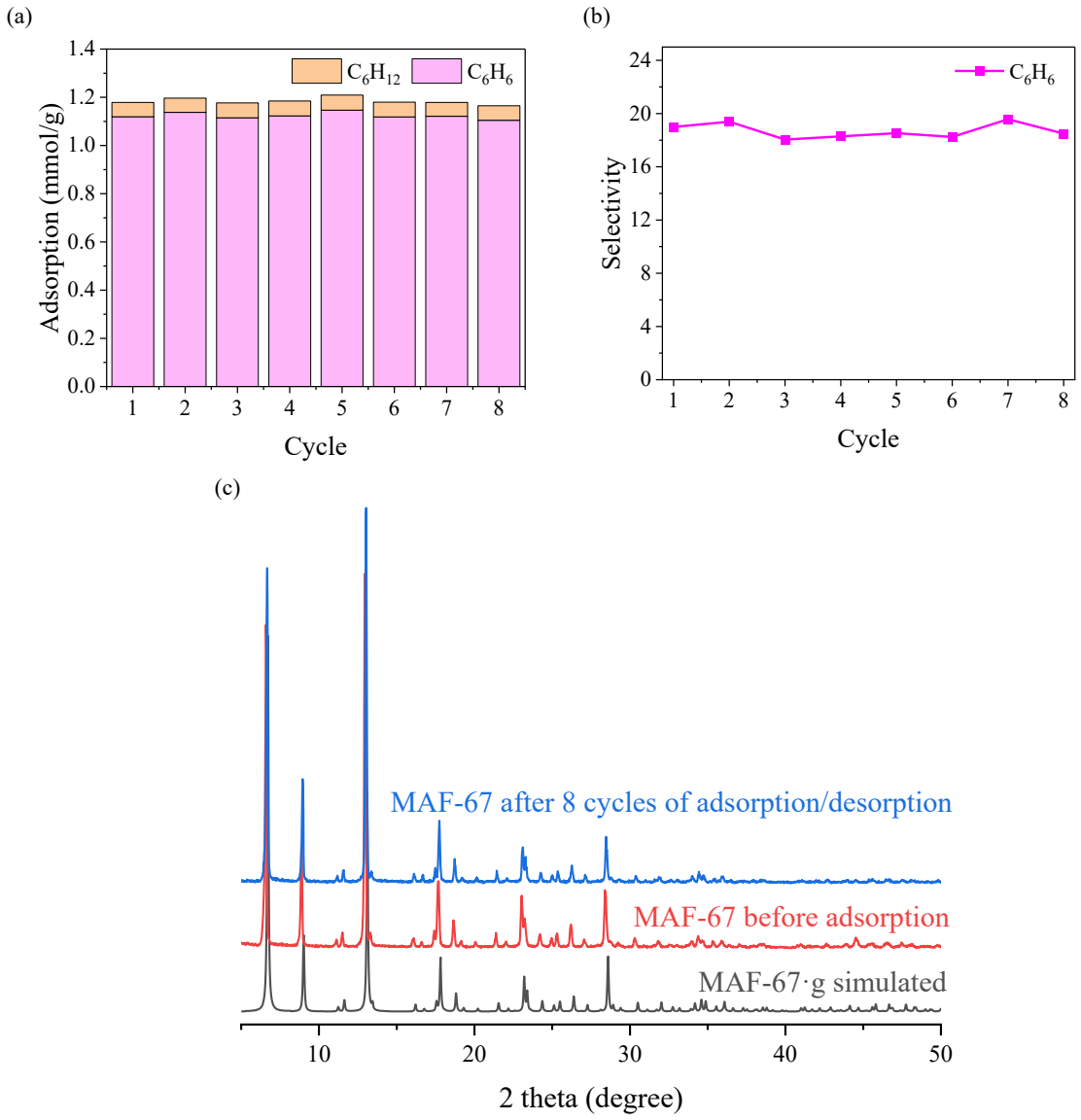

Figure S14. Sorption cycling of small-particle MAF-67 after soaking in benzene/cyclohexane for 5 seconds (0.083 min). (a) Adsorption capacity, (b) selectivity, and (c) comparison of PXRD patterns under different conditions.

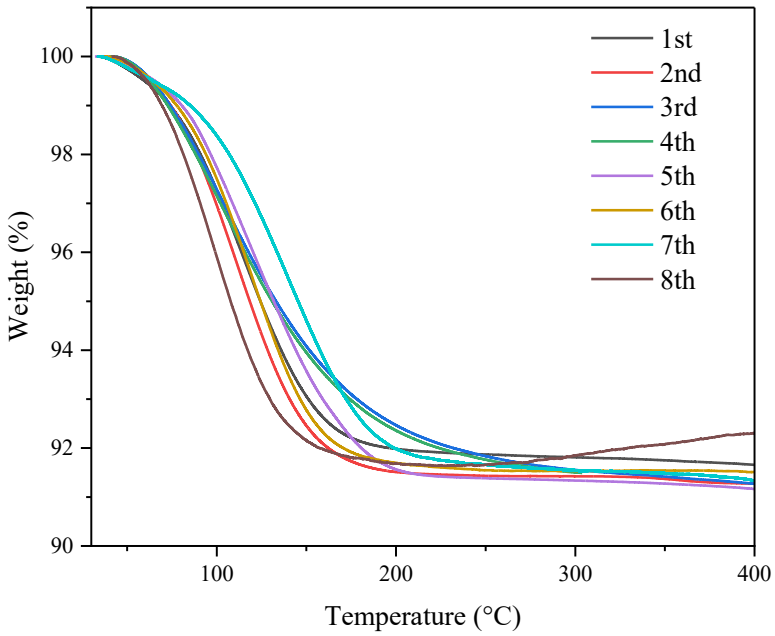

Figure S15. TG analysis of MAF-67 after multicycle soaking in benzene/cyclohexane for 5 seconds (0.083 min).

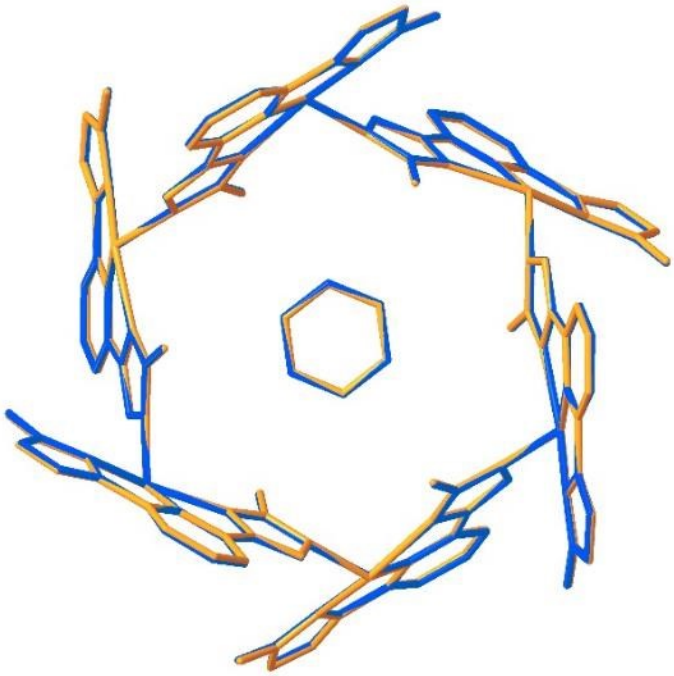

Figure S16. Overlaps of DFT-simulated structure of benzene-loaded MAF-67 (orange) and as-synthesized MAF-67·1/3(C_6H_6) (blue, disordered C_6H_6 in the cavity is omitted).

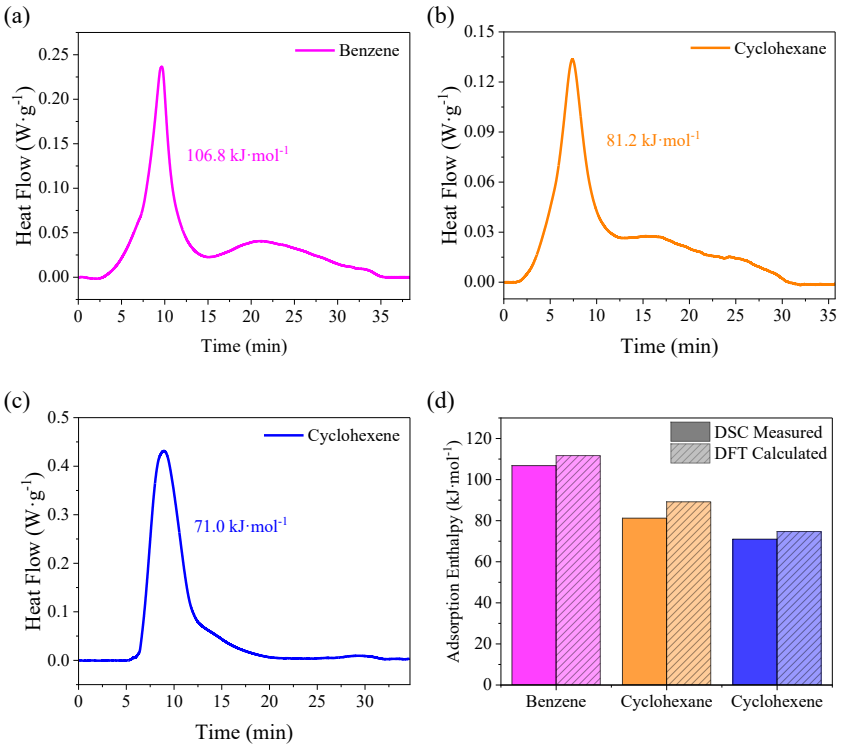

Figure S17. Sorption enthalpies of MAF-67 for (a) benzene, (b) cyclohexane and (c) cyclohexene by DSC analyses. (d) Comparison of sorption enthalpies with corresponding results from DFT calculation.

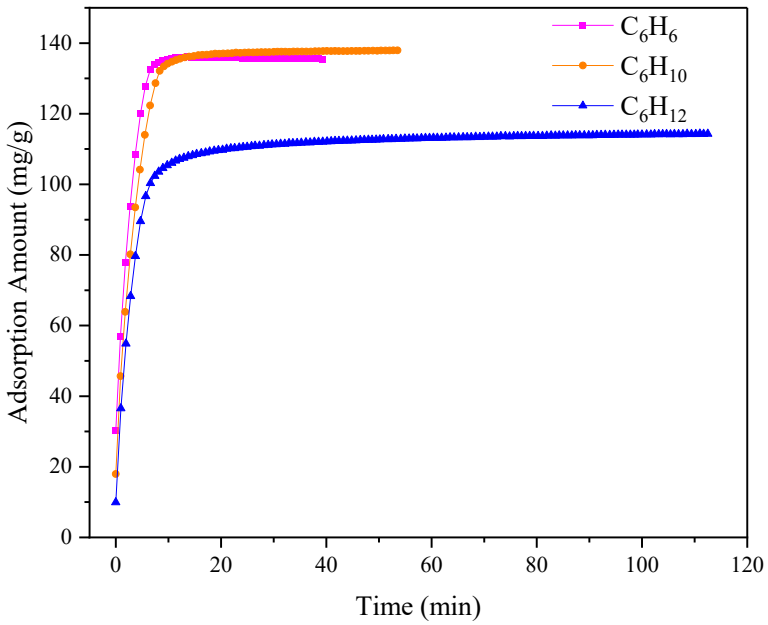

Figure S18. Adsorption kinetics curves for single-component vapor of benzene, cyclohexane or cyclohexene.

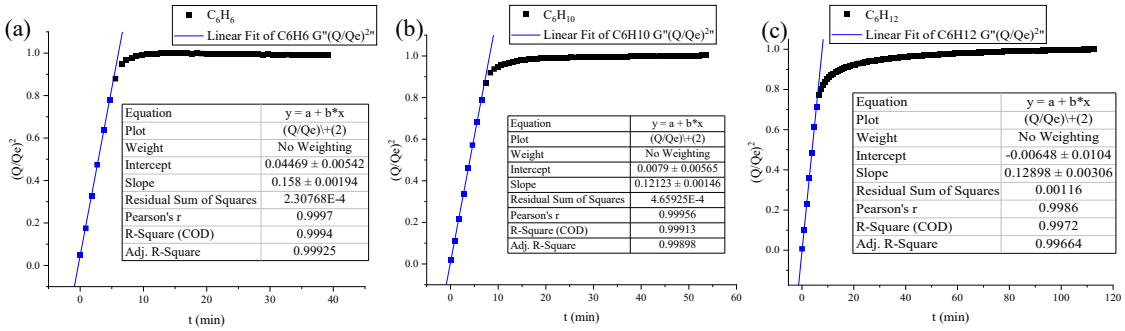

Figure S19. Linear fitting of adsorption kinetics of MAF-67 for (a) benzene, (b) cyclohexane and (c) cyclohexene by using the intraparticle diffusion equation (base on Equation (8), that can identify the time range during adsorption process controlled by intraparticle diffusion.

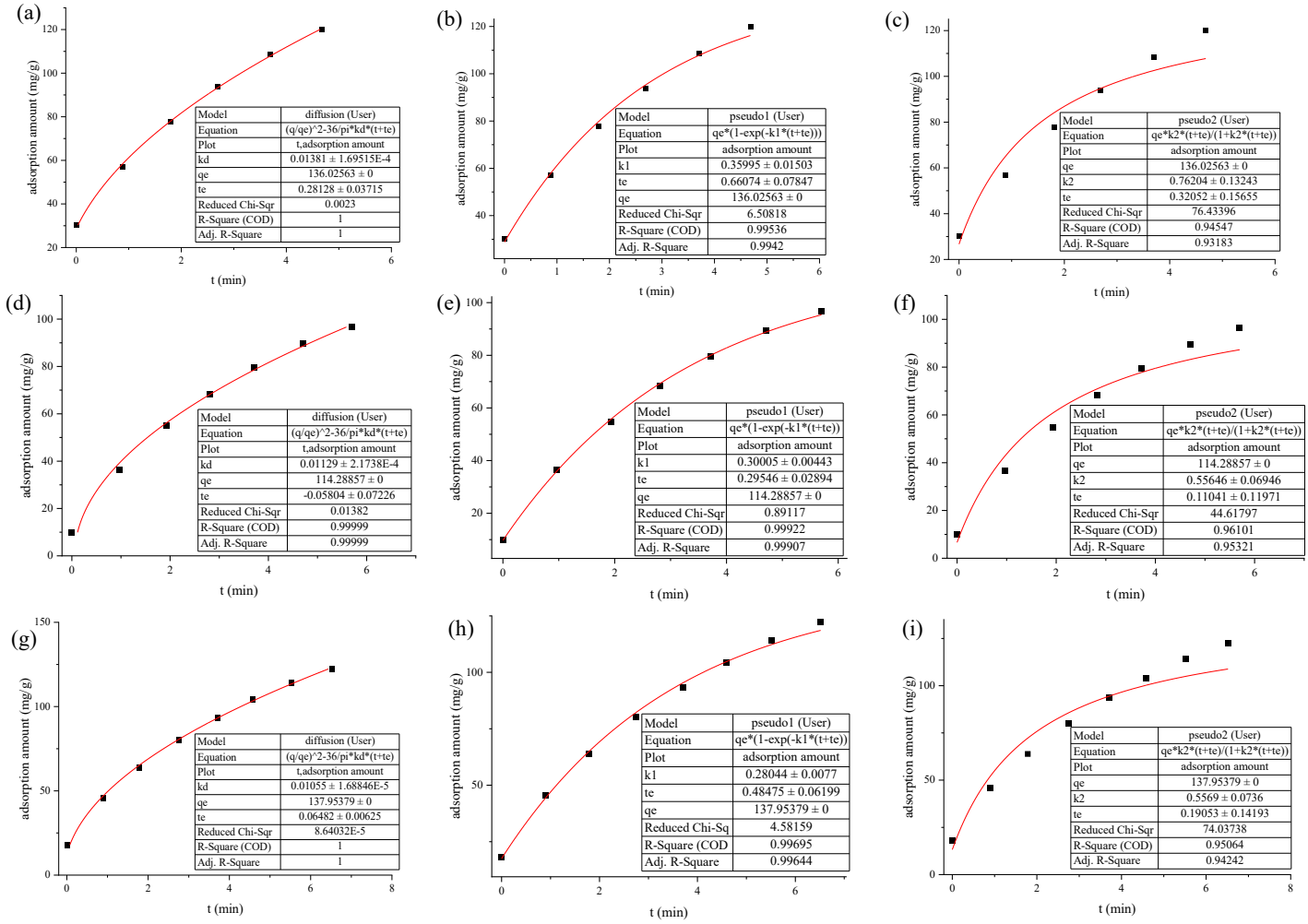

Figure S20. Nonlinear fitting of different models (Equations (8), 10, and (12)) in the first step (obtained from Figure S19) of the vapor adsorption kinetics curves for (a-c) benzene, (d-f) cyclohexane and (g-i) cyclohexene in MAF-67. The data were fitted by intraparticle diffusion model (left, $R^2 > 0.99999$), pseudo-first order model (middle) and pseudo-second order model (right), respectively.

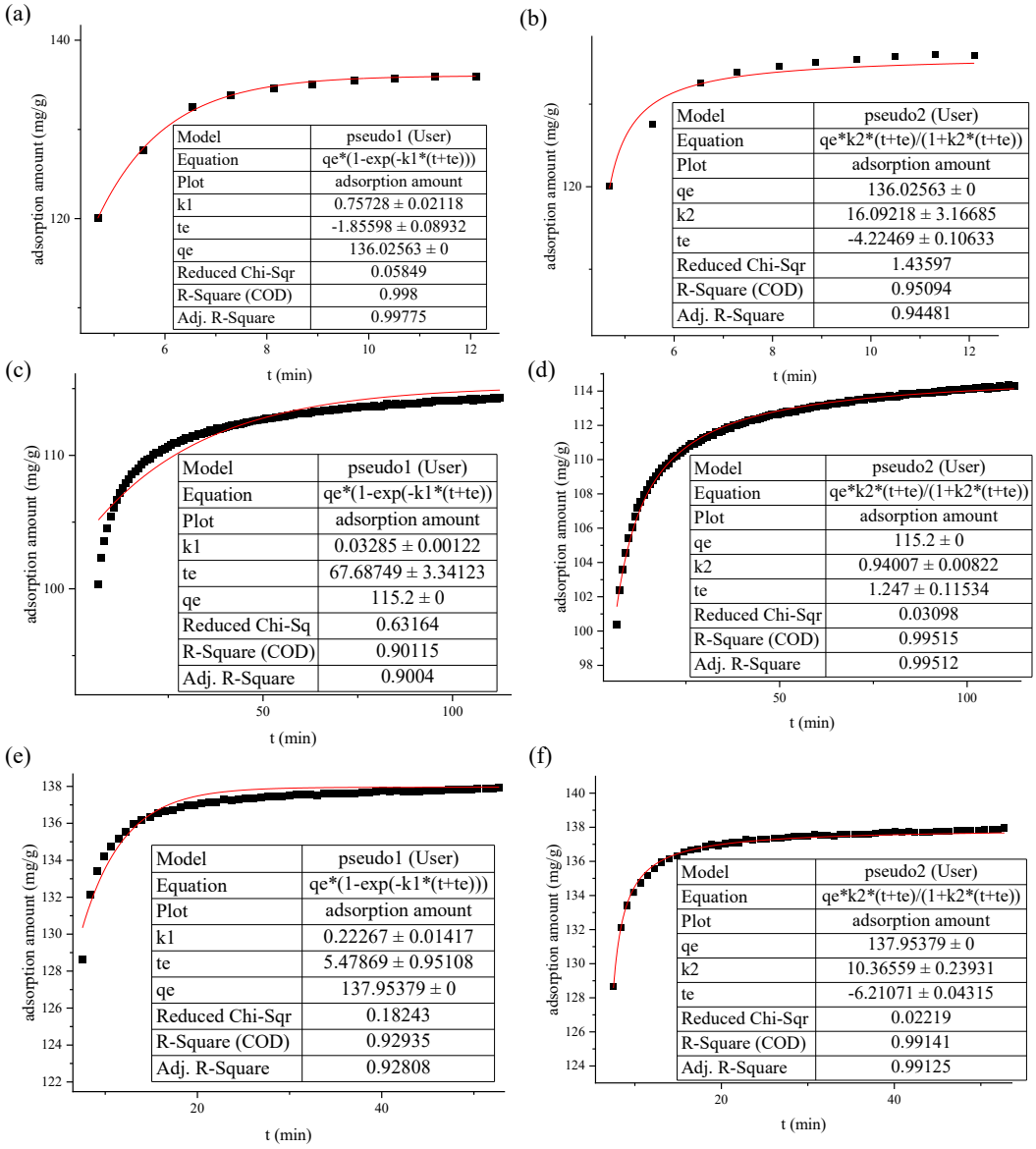

Figure S21. Nonlinear fitting of pseudo-first order and pseudo-second order models (Equations (10) and (12)) in the second step of the vapor adsorption kinetics curves for (a-b) benzene, (c-d) cyclohexane and (e-f) cyclohexene in MAF-67. The data were fitted by pseudo-first order (left) and pseudo-second order (right), respectively. The fitting results in (a), (d), and (f), showing $R^2 > 0.99$, which is significantly better than that of (b, c, e).

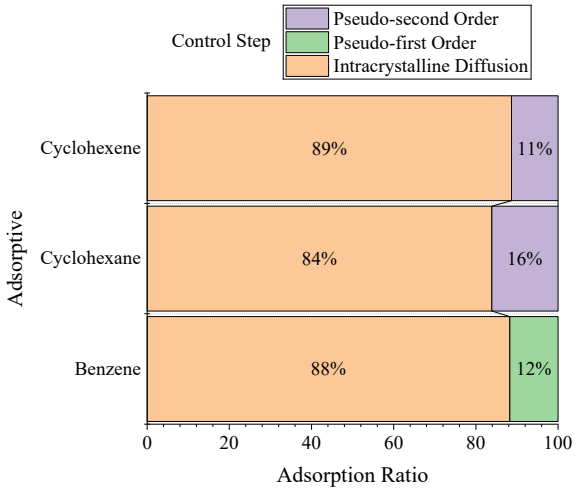

Figure S22. Contribution comparison of different diffusion steps during adsorption of cyclic C6s (summarized from Figure S19-Figure S21).

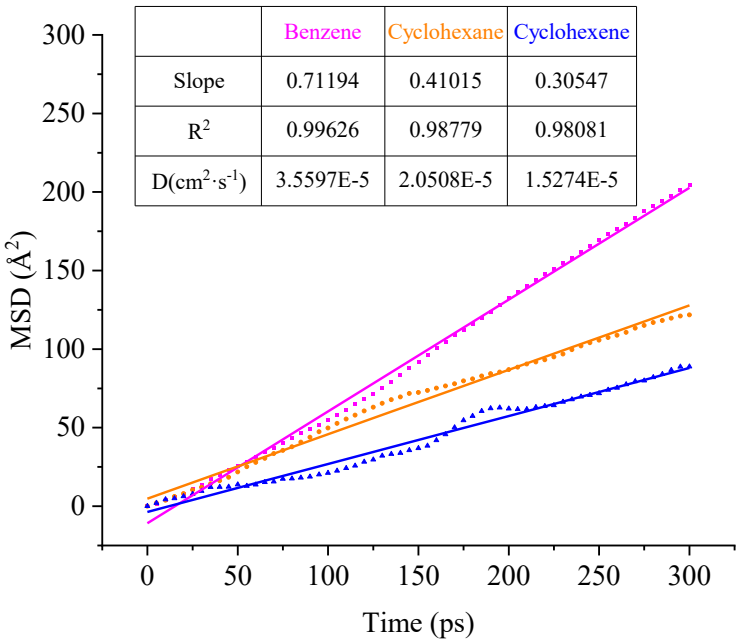

Figure S23. MD simulations of the intraparticle diffusion of benzene (pink), cyclohexane (orange), and cyclohexene (blue) in MAF-67.

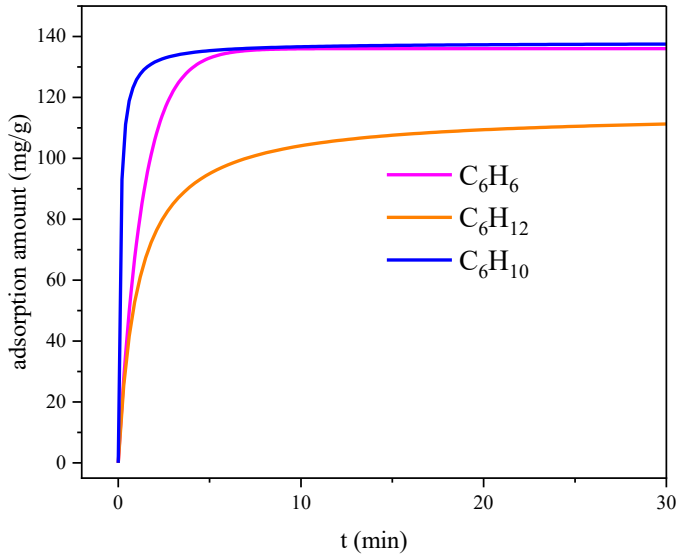

Figure S24. Simulated adsorption kinetics dominated solely by surface adsorption reactions after excluding the influence of intraparticle diffusion (based on equations from Figure S21(a), (d), and (f), t_{eff} is set to 0).

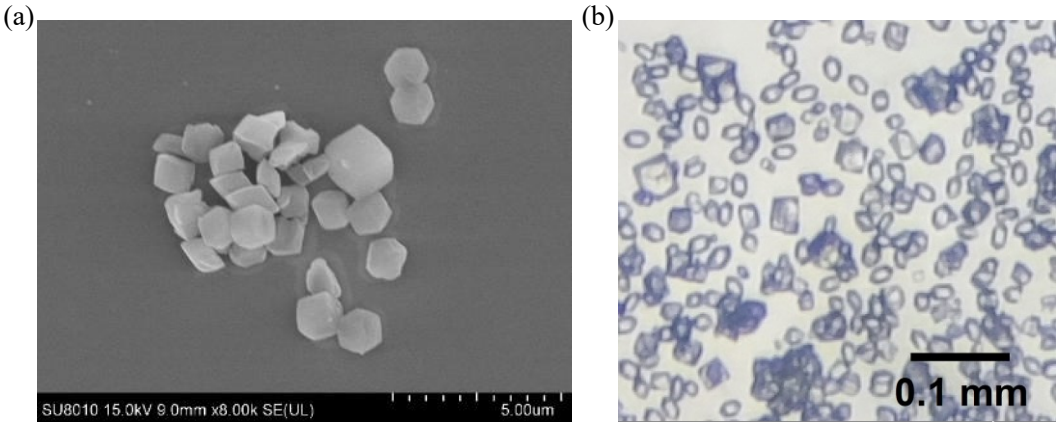

Figure S25. (a) Small-particle and (b) large-particle samples of MAF-67·g.

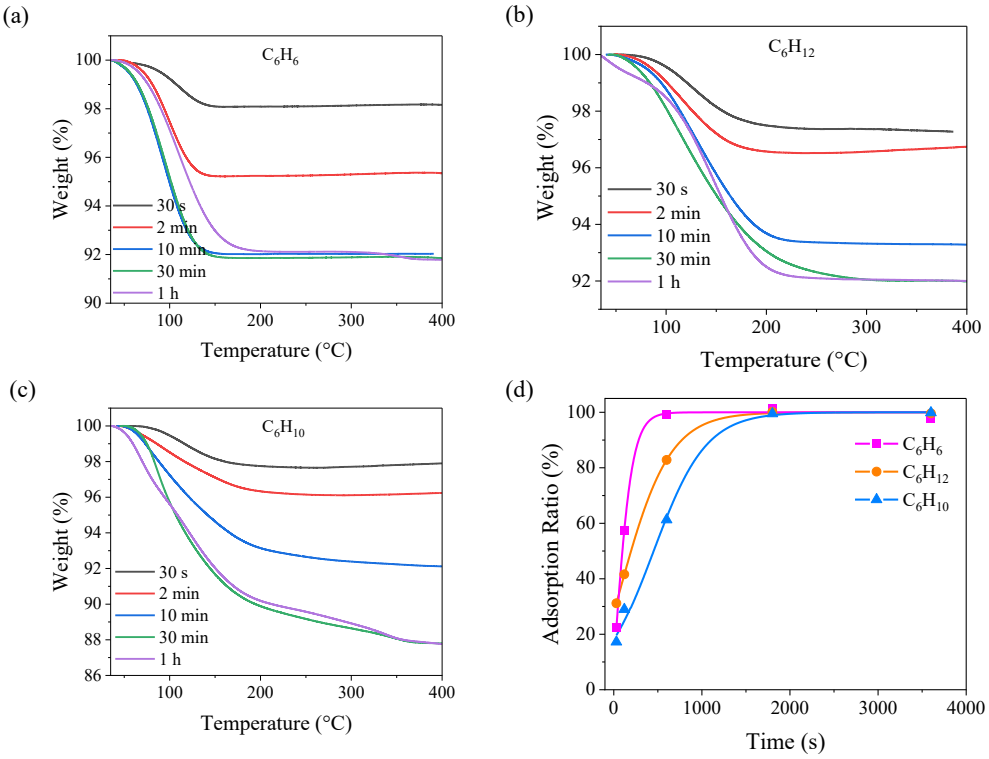

Figure S26. TG analyses of large-particle samples for adsorption of liquid-phase (a) benzene, (b) cyclohexane and (c) cyclohexene. (d) Corresponding adsorption kinetics.

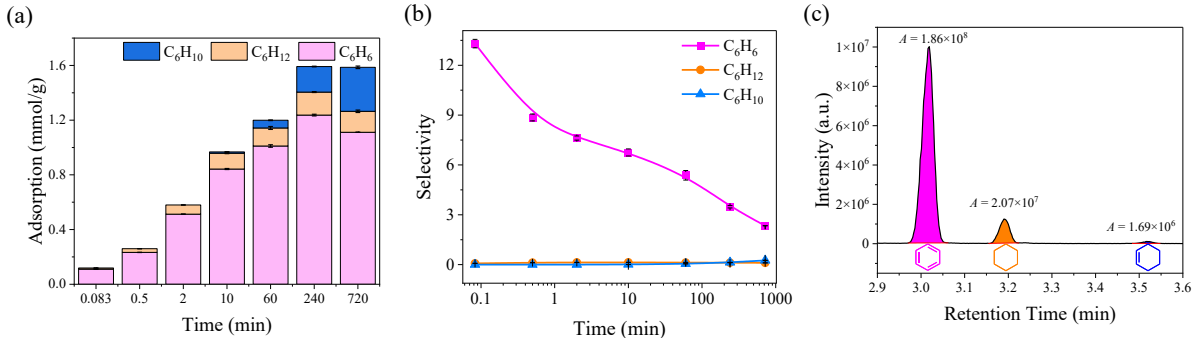

Figure S27. Competitive adsorption kinetics of liquid benzene/cyclohexane/cyclohexene mixtures (1:1:1) in large-particle sample of MAF-67. (a) Adsorption amounts, (b) selectivities and (c) GC-MS results for the sample at 10 min.

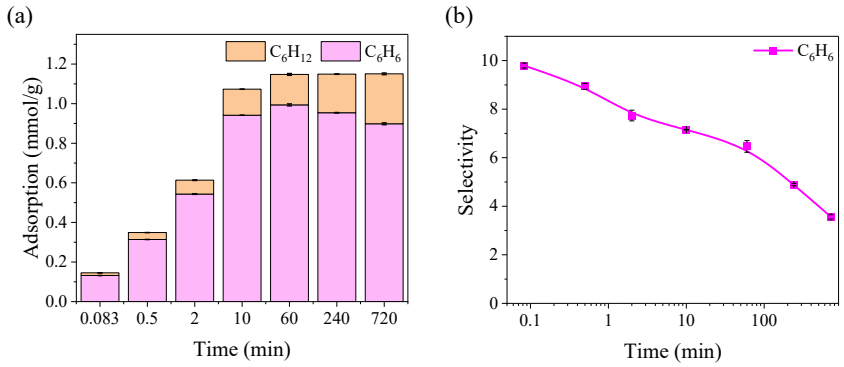

Figure S28. Competitive adsorption kinetics of liquid benzene/cyclohexane mixtures (1:1) in large-particle sample of MAF-67. (a) Adsorption amounts and (b) selectivity.

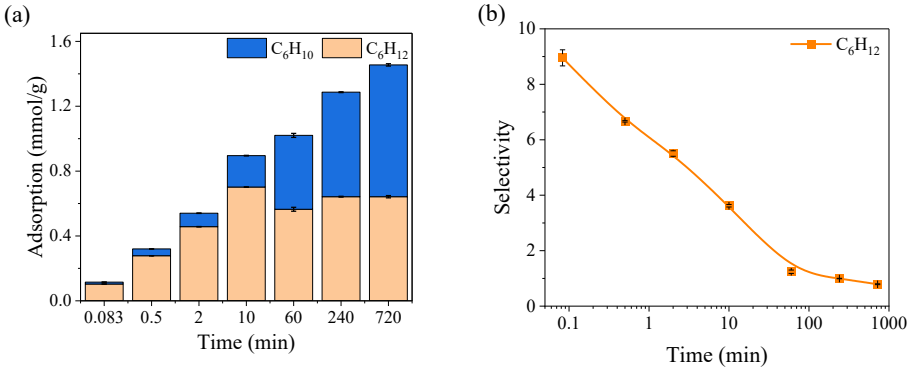

Figure S29. Competitive adsorption kinetics of liquid cyclohexane/cyclohexene mixtures (1:1) in large-particle sample of MAF-67. (a) Adsorption amounts and (b) selectivity.

Table S1. Crystallographic data of MAF-67.

Crystal structure information		
Compound	MAF-67·g	MAF-67·1/3(C_6H_6)
Formula	$C_{11}H_9N_7Zn$	$C_{13}H_{11}N_7Zn$
Formula weight	304.62	330.66
Crystal system	trigonal	trigonal
Space Group	*R*-3	*R*-3
a (Å)	26.3223(7)	26.4056(9)
c (Å)	10.8595(3)	10.8599(4)
V (Å^3)	6516.1(4)	6557.6(5)
T (K)	150.02(15)	149.99(10)
Z	18	18
R_1 [I > 2σ(I)][a]	0.0383	0.0423
wR_2 [I > 2σ(I)][b]	0.1007	0.1102
R_1 (all data)	0.0463	0.0561
wR_2 (all data)	0.1048	0.1191
GOF	1.156	1.036
Completeness (%)	97.7	98.6
Void ratio[c] (%)	25.1	/
D_c (g·cm^{-3})	1.397	1.507
Pore volume (cm^3·g^{-1})	0.182	/

[a] $R_1=\sum||F_o|-|F_c||/\sum|F_o|$

[b] $wR_2=[\sum w(F_o^2-F_c^2)^2/\sum w(F_o^2)^2]^{1/2}$

[c] Calculated by PLATON using probe radius of 1.2 Å

Table S2. Comparison on the adsorption of benzene in various benzene-selective adsorbents (non-MOF materials are highlighted in orange) for equimolar mixtures of benzene/cyclohexane or benzene/cyclohexene.

Adsorbent	Adsorption Time	Type	C_6H_6 adsorbed amount ($mmol \cdot g^{-1}$) [a]		$S_{C_6H_6/C_6H_{12}}$	$S_{C_6H_6/C_6H_{10}}$	Ref.
[Zn(bmtzpy)]	5 s[b]	liquid	1.13[c]	1.10[d]	18.7	19.1	**This work**
	30 s[b]		1.12[c]	1.48[d]	18.0	18.3	
[Zn(μ_4-TCNQ-TCNQ)bpy]	5 h	vapor	3.6		19	/	[6]
[Mn(μ_4-TCNQ-TCNQ)bpy]	24 h	vapor	3.7		19	/	[7]
[ZnL], H_2L = (R,R)-(−)-N,N′-bis(3-tert-butyl-5-(4-ethynylpyridyl)salicylidene)-1,2-diaminocyclohexane)	1 h	liquid	1.51		32.3	/	[8]
$[Li_2Zn_2(R\text{-}bdc)_3(bpy)]$	1 d	liquid	2.9		17	/	[9]
CID-23	24 h	vapor	1.20		25	/	[10]
Et_3NH@ZnPzC	24 h	liquid	/		14	/	[11]
$[Zn_4(EGO_2)_2(tdc)_2(dabco)]$	5 d	liquid	0.92		92	/	[12]
MAF-stu-13	18 h	liquid	2.59		166	/	[13]
MFM-300(Sc)	24 h	liquid	3.02		166	/	[14]
	20 min (single-component) [b]	vapor				/	
$Ag_3L_2(SbF_6)_3$ L = 3,6-bis[2-(4-oxide-quinoxaline)-yl]-4,5-diaza-3,5-octadiene	1 week	liquid/vapor	0.64		∞[e]	∞[e]	[15]
T[5]-$(OMe)_5$	5 h[b]	vapor	1.3		12	/	[16]
hybrid[3]arene	9 h[b]	vapor	1.4		39	/	[17]
L^H-$Au_{10}S_4$-Cl	24 h	liquid	0.18		23	/	[18]
Naphthotube $C_{56}H_{50}N_2O_{12}$	1.5 h[b]	vapor	1.6		37[f]	7.8[f]	[19]

[a] In this work, the practical adsorption amount of benzene in mixture adsorption was experimentally measured and used here; whereas for those values were not reported in the literatures, then single-component saturated adsorption capacity were used.

[b] Adsorption kinetics were experimentally measured.

[c] Co-adsorption of benzene/cyclohexane.

[d] Co-adsorption of benzene/cyclohexene.

[e] The other component was not detected.

[f] Obtained from reported data in literatures.

Table S3. Host-guest interactions at the major binding sites in MAF-67.

	Type	Hydrogen bonds(H···A/D···A) distance / Å					
C_6H_6	C-H_{guest}···N_{host}	2.765/3.764	2.769/3.767	2.777/3.774	2.792/3.790	2.793/3.791	2.801/3.802
C_6H_{12}	C-H_{guest}···π_{host}	2.812/3.728	2.829/3.805				
C_6H_{10}	C-H_{guest}···N_{host}	2.837/3.829	2.842/3.813	2.869/3.821	2.909/3.818	3.005/3.971	3.038/4.019

Table S4. Average binding energy of MAF-67 at different diffusion steps of C_6H_6/C_6H_{12}/C_6H_{10} adsorption.

Binding energy for different C6s (kJ mol^{-1})	Average number of adsorbed molecules per cavity			
	0~1	1~2	1~3	Total average
C_6H_6	129.3	94.1		111.7
C_6H_{12}	107.5	70.9		89.2
C_6H_{10}	123.4		52.3	74.7

Table S5. Adsorption rate coefficients for benzene/cyclohexane/cyclohexene in MAF-67 (based on Figure S20-S21).

	Benzene	Cyclohexane	Cyclohexene
k_D (min^{-1})	0.01381	0.01129	0.01055
k_1 (min^{-1})	0.7696		
k_2^* (min^{-1})		0.9401	10.3656

Table S6. Data of vapor adsorption kinetics in MAF-67.

Benzene					
Time (min)	Adsorption Amount (mg/g)	Time (min)	Adsorption Amount (mg/g)	Time (min)	Adsorption Amount (mg/g)
0	30.28562	14.38333	136.08088	28.08333	135.69416
0.88333	56.95818	15.18333	136.02563	28.86667	135.62787
1.8	77.80233	16.06667	136.02563	29.68333	135.68311
2.68333	93.70753	16.91667	136.02563	30.46667	135.58367
3.7	108.55754	17.68333	135.96486	31.21667	135.63339
4.68333	120.05967	18.45	135.97591	31.98333	135.58367
5.56667	127.62278	19.21667	135.92067	32.7	135.57262
6.53333	132.55069	20.03333	135.91514	33.48333	135.63891
7.28333	133.87106	20.81667	135.86542	34.26667	135.57262
8.13333	134.59477	21.65	135.84885	35.08333	135.58367
8.88333	135.07541	22.48333	135.81018	35.91667	135.52842
9.71667	135.46765	23.21667	135.80465	36.76667	135.57814
10.5	135.74941	24.1	135.73836	37.6	135.53395
11.3	135.96486	24.81667	135.68864	38.48333	135.53395
12.1	135.92067	25.61667	135.69969	39.16667	135.46213
12.81667	136.02011	26.5	135.69416		
13.56667	136.13613	27.3	135.68864		
Cyclohexane					
Time (min)	Adsorption Amount (mg/g)	Time (min)	Adsorption Amount (mg/g)	Time (min)	Adsorption Amount (mg/g)
0	9.92054	39.31667	112.07045	77.1	113.62313
0.96667	36.54351	40.13333	112.12036	77.88333	113.67304
1.93333	54.88735	40.9	112.18135	78.65	113.67858
2.81667	68.31806	41.66667	112.27562	79.4	113.72295
3.71667	79.67482	42.4	112.28671	80.25	113.67858
4.7	89.54545	43.21667	112.34217	81.06667	113.67304
5.7	96.64343	43.98333	112.33108	81.88333	113.73404
6.58333	100.35878	44.81667	112.38653	82.71667	113.84494
7.38333	102.36063	45.65	112.45307	83.51667	113.77285
8.15	103.56951	46.43333	112.51407	84.25	113.82831
8.93333	104.56766	47.21667	112.56952	85.01667	113.84494
9.76667	105.405	47.98333	112.61943	85.86667	113.82831
10.61667	106.07044	48.68333	112.62498	86.65	113.83385
11.36667	106.68596	49.45	112.66379	87.4	113.88376

12.1	107.17395	50.16667	112.67488	88.16667	113.89485
12.93333	107.5233	50.86667	112.7747	89.01667	113.9004
13.75	107.95029	51.73333	112.79134	89.88333	113.89485
14.56667	108.22756	52.46667	112.78025	90.65	113.88376
15.35	108.57691	53.26667	112.84124	91.41667	113.95585
16.23333	108.79872	54.13333	112.84124	92.2	113.94476
17.05	109.00944	54.93333	112.9466	93	113.99467
17.83333	109.28671	55.73333	112.9466	93.86667	113.9503
18.68333	109.51407	56.51667	113.01315	94.66667	114.0113
19.48333	109.67488	57.23333	112.99651	95.45	114.06675
20.28333	109.78024	58.08333	113.0686	96.21667	114.06675
21.05	110.07414	58.83333	113.12405	97	114.06675
21.83333	110.1795	59.6	113.11851	97.76667	114.06121
22.6	110.23495	60.35	113.16842	98.51667	114.06121
23.43333	110.40686	61.08333	113.16287	99.2	114.11112
24.18333	110.51222	61.91667	113.16842	100	114.11112
24.95	110.62867	62.75	113.21832	100.86667	114.12221
25.78333	110.79503	63.5	113.28487	101.68333	114.10557
26.46667	110.90039	64.28333	113.27932	102.4	114.17766
27.28333	110.90039	65.15	113.29041	103.18333	114.16102
28.15	111.0612	66	113.34587	103.93333	114.17766
28.93333	111.17765	66.76667	113.34032	104.66667	114.22202
29.68333	111.29411	67.53333	113.34032	105.41667	114.12221
30.51667	111.33847	68.4	113.45677	106.15	114.22757
31.3	111.44383	69.18333	113.39023	106.95	114.16657
32.11667	111.44937	69.95	113.45123	107.78333	114.16102
32.91667	111.61573	70.8	113.51222	108.56667	114.28302
33.65	111.62682	71.58333	113.50668	109.4	114.23311
34.45	111.67673	72.4	113.50113	110.21667	114.23311
35.25	111.77655	73.18333	113.61759	110.98333	114.34402
36.13333	111.88745	74.01667	113.61204	111.71667	114.27748
36.93333	111.832	74.81667	113.55104	112.51667	114.28857
37.73333	112.01499	75.61667	113.62313		
38.51667	111.99836	76.36667	113.66749		
Cyclohexene					
Time (min)	Adsorption Amount (mg/g)	Time (min)	Adsorption Amount (mg/g)	Time (min)	Adsorption Amount (mg/g)
0	17.95468	19.65	136.95569	37.85	137.67099

0.9	45.67962	20.41667	137.06104	38.61667	137.68208
1.78333	63.87828	21.28333	137.11649	39.38333	137.7209
2.75	80.175	22.06667	137.12204	40.11667	137.77635
3.7	93.47743	22.85	137.29393	40.91667	137.7209
4.58333	104.17926	23.66667	137.23848	41.65	137.79298
5.51667	114.00498	24.5	137.29393	42.38333	137.7209
6.51667	122.31137	25.26667	137.33275	43.21667	137.73199
7.53333	128.63821	26.08333	137.33829	44.01667	137.73199
8.35	132.13155	26.88333	137.3882	44.81667	137.78744
9.13333	133.41244	27.65	137.44919	45.63333	137.77635
9.85	134.18874	28.41667	137.45474	46.36667	137.78744
10.66667	134.73769	29.18333	137.45474	47.23333	137.83734
11.45	135.18129	30.01667	137.50464	48.01667	137.83734
12.21667	135.5639	30.73333	137.56564	48.86667	137.84289
13.08333	135.9465	31.46667	137.55455	49.68333	137.8318
13.95	136.1683	32.21667	137.56009	50.4	137.88725
14.83333	136.3402	33	137.50464	51.26667	137.89279
15.68333	136.56754	33.75	137.61554	52.03333	137.88725
16.46667	136.66735	34.53333	137.61554	52.73333	137.95379
17.28333	136.7228	35.38333	137.61554	53.53333	137.95379
18.13333	136.85034	36.2	137.62109		
18.88333	137.00005	37.06667	137.61554		

4. References

1 S. Bahceci, H. Yueksek and M. Serdar, *ChemInform*, 2005, **36**, chin.200528140.

2 A. Torres-Knoop, R. Krishna and D. Dubbeldam, *Angew. Chem., Int. Ed.*, 2014, **53**, 7774–7778.

3 W. Rudzinski and W. Plazinski, *Appl. Surf. Sci.*, 2007, **253**, 5827–5840.

4 J.-P. Simonin, *Chem. Eng. J.*, 2016, **300**, 254–263.

5 J. Kärger, D. M. Ruthven and D. N. Theodorou, *Diffusion in Nanoporous Materials*, Wiley, 2012.

6 S. Shimomura, S. Horike, R. Matsuda and S. Kitagawa, *J. Am. Chem. Soc.*, 2007, **129**, 10990–10991.

7 S. Shimomura, R. Matsuda and S. Kitagawa, *Chem. Mater.*, 2010, **22**, 4129–4131.

8 G. Li, C. Zhu, X. Xi and Y. Cui, *Chem. Commun.*, 2009, 2118–2120.

9 A. A. Sapianik, K. A. Kovalenko, D. G. Samsonenko, M. O. Barsukova, D. N. Dybtsev and V. P. Fedin, *Chem. Commun.*, 2020, **56**, 8241–8244.

10 Y. Hijikata, S. Horike, M. Sugimoto, H. Sato, R. Matsuda and S. Kitagawa, *Chem. Eur. J.*, 2011, **17**, 5138–5144.

11 J.-H. Wang, D. Luo, M. Li and D. Li, *Cryst. Growth & Des.*, 2017, **17**, 3387–3394.

12 A. A. Lysova, D. G. Samsonenko, P. V. Dorovatovskii, V. A. Lazarenko, V. N. Khrustalev, K. A. Kovalenko, D. N. Dybtsev and V. P. Fedin, *J. Am. Chem. Soc.*, 2019, **141**, 17260–17269.

13 C.-R. Ye, W.-J. Wang, W. Chen, Y. Xiao, H.-F. Zhang, B.-L. Dai, S.-H. Chen, X.-D. Wu, M. Li and X.-C. Huang,

Angew. Chem., Int. Ed., 2021, **60**, 23590–23595.

14 Y. Han, Y. Chen, Y. Ma, J. Bailey, Z. Wang, D. Lee, A. M. Sheveleva, F. Tuna, E. J. L. McInnes, M. D. Frogley, S. J. Day, S. P. Thompson, B. F. Spencer, M. Nikiel, P. Manuel, D. Crawshaw, M. Schröder and S. Yang, *Chem*, 2023, **9**, 739–754.

15 J.-Y. Cheng, P. Wang, J.-P. Ma, Q.-K. Liu and Y.-B. Dong, *Chem. Commun.*, 2014, **50**, 13672–13675.

16 W. Yang, K. Samanta, X. Wan, T. U. Thikekar, Y. Chao, S. Li, K. Du, J. Xu, Y. Gao, H. Zuilhof and A. C.-H. Sue, *Angew. Chem., Int. Ed.*, 2020, **59**, 3994–3999.

17 J. Zhou, G. Yu, Q. Li, M. Wang and F. Huang, *J. Am. Chem. Soc.*, 2020, **142**, 2228–2232.

18 L.-Y. Yao and V. W.-W. Yam, *J. Am. Chem. Soc.*, 2021, **143**, 2558–2566.

19 H. Yao, Y.-M. Wang, M. Quan, M. U. Farooq, L.-P. Yang and W. Jiang, *Angew. Chem., Int. Ed.*, 2020, **59**, 19945–19950.